Preparation and Lithium Storage Performances of Mesoporous Fe3O4@C Microcapsules

6 AUTHORS, INCLUDING:

Letao Yang
Rutgers, The State University of New Jersey

7 PUBLICATIONS   **186** CITATIONS

SEE PROFILE

Liwei Su
Zhejiang University of Technology

33 PUBLICATIONS   **912** CITATIONS

SEE PROFILE

Zhen Zhou
Nankai University

213 PUBLICATIONS   **6,996** CITATIONS

SEE PROFILE

# Preparation and Lithium Storage Performances of Mesoporous Fe₃O₄@C Microcapsules

S. M. Yuan, J. X. Li, L. T. Yang, L. W. Su, L. Liu, and Z. Zhou*

Institute of New Energy Material Chemistry, Key Laboratory of Advanced Energy Materials Chemistry (Ministry of Education), and Tianjin Key Laboratory of Environmental Remediation and Pollution Control, Nankai University, Tianjin 300071, People's Republic of China

Ⓢ *Supporting Information*

ABSTRACT: Fe₃O₄@C microcapsules were prepared using carbon-coated α-FeOOH nanorods as precursors, which were synthesized via two-step hydrothermal reactions. During the subsequent sintering procedure, α-FeOOH was reduced to Fe₃O₄ by carbon, accompanied by the formation of mesopores. In Fe₃O₄@C microcapsules, mesoporous Fe₃O₄ nanorods are coated with amorphorous carbon layers. The Fe₃O₄/C composites with such special structures demonstrate high specific capacity and good cyclic stability as anode materials in Li test cells.

KEYWORDS: microcapsules, mesoporous materials, nanorods, Fe₃O₄, lithium ion batteries
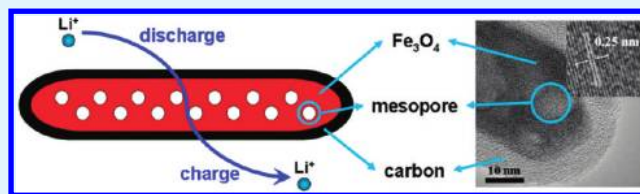
■ INTRODUCTION

The ever-growing demand for high-performance power sources has prompted tremendous research efforts toward developing new electrode materials for next-generation lithium-ion batteries (LIBs).[1−3] With unique characteristics, transition-metal oxides (such as Fe₂O₃, Fe₃O₄, Co₃O₄, and NiO) with various nanostructures have been extensively explored as LIB anode materials.[4−12] One of the promising oxides for use as a LIB anode material is magnetite (Fe₃O₄), which has high theoretical capacity (∼928 mAh g⁻¹, which is ∼3 times that of conventional graphite), low cost, good stability, and environmental friendliness. Furthermore, Fe₃O₄ is among the limited transition-metal oxides with high electronic conductivity, which is extraordinarily important for LIB materials.[13,14] However, there are still obstacles to using Fe₃O₄ as a LIB anode material. First, the lithium storage mechanism in Fe₃O₄ can be interpreted as

$$Fe_3O_4 + 8Li^+ + 8e^- \longrightarrow 3Fe + 4Li_2O$$
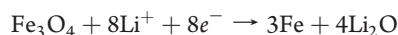
Thus, fundamental changes occur to the structure after the lithium inclusion. Second, the generated Fe nanograins (<5 nm) with large specific surface have high catalytic activity in some irreversible reactions and cause poor capacity retention over extended cycles.[2] Lastly, the solid electrolyte interphase (SEI) film on Fe₃O₄ anodes may be destroyed because of the large volume change, and the repeated formation/decomposition of the SEI film consumes the Li ions supplied by the cathodes and also leads to poor cyclic performance.[15−17]

An amazing technique to overcome the above-mentioned obstacles is to encapsulate the oxide core by a carbon shell, i.e., to synthesize core−shell nanoparticles. The carbon coating significantly improves the electrochemical performance of active materials by providing high electronic conductivity, good lithium permeability, and flexible accommodation of volume change.[18−22] Carbon-coated Fe₃O₄ nanorods, nanospindles, and nanowires have been synthesized and presented better electrochemical performance.[9,23−26] Mesoporous structure is another strategy for improving the electrochemical performance of oxide anode materials, which can buffer volume changes, to some extent, with the mesopores,[27] while the increased material/electrolyte interfaces, accompanied by the mesoporous materials, can raise the risk of side reactions.[4] Thus, an interesting idea arises: *what about skillfully combining a mesoporous structure and carbon encapsulation simultaneously in one material system?* The mesopore structure can supply a cushion space for the volume changes, and the carbon shell can protect the active materials from directly contacting with the electrolyte. In the usual way, the first step is to prepare the mesoporous materials and then coat the materials with carbon; however, the mesopores may be blocked or even filled by carbon. To avoid this result, here, we propose a special route, using α-FeOOH nanorods coated with carbon layers as precursors, to prepare Fe₃O₄@C microcapsules, in which mesopores are generated during the sintering procedure after the carbon coating.

■ EXPERIMENTAL SECTION

Preparation of Fe₃O₄@C Miscrocapsules. In a typical synthesis, α-FeOOH was prepared using FeCl₃·6H₂O and NaOH as

starting materials. Twenty-five milliliters of a distilled water solution containing 1.35 g of $FeCl_3 \cdot 6H_2O$ was slowly added to 75 mL of a distilled water solution containing 1.00 g of NaOH with magnetic stirring for 30 min. The resulting solution was then transferred to a 100-mL Teflon-lined stainless steel autoclave and heated at 180 °C for 24 h. After the autoclave cooled, the sample was divided into two parts: one was dried in the oven at 100 °C for 12 h and further heated at 500 °C for 4 h in an argon atmosphere; the other (1.0 g of as-prepared α-FeOOH) was transferred to a clear solution containing 2.0 g of glucose dissolved in a solution containing 35 mL of deionized water and 10 mL of ethanol. The mixture was placed in a 50-mL Teflon-sealed autoclave, ultrasonically dispersed for 30 min, and maintained at 180 °C in a drying oven for 2 h. The product was centrifuged and washed with deionized water and absolute ethanol for at least five times and dried in an oven at 100 °C for 12 h. Finally, the samples were sintered at 500 °C for 4 h in flowing argon.

Sample Characterization. The samples were characterized by X-ray diffraction (XRD) (using a Rigaku D/Max III diffractometer with Cu Kα radiation, $\lambda = 1.5418$ Å), scanning electron microscopy (SEM) (using a FEI Nanosem 430 field-emission gun scanning electron microscope), transmission electron microscopy (TEM) (using a FEI Tecnai G^2F-20 field-emission gun transmission electron microscope), energy-dispersive X-ray spectroscopy (EDS) (using a EDAX Genesis XM2 APEX 60 SEM X-ray energy-dispersive spectrometer), thermogravimetric/differential thermal analysis (TG-DTA) (using a Rigaku PTC-10A TG-DTA analyzer), and Raman spectrum (using a Renishaw inVia Raman spectrometer). The Brunauer−Emmett−Teller (BET) nitrogen physisorption experiments (mesoporous analysis) were carried out on a Quantachrome NOVA 2000e sorption analyzer. The specific surface areas (S_{BET}) of the samples were calculated following the multipoint BET procedure. The pore-size distributions were determined using the Barrett−Joyner−Halenda (BJH) method.

Electrochemical Tests. Electrochemical performances of the samples were evaluated in Li test cells. The working electrodes were comprised of active material, acetylene black, and polytetrafluoroethylene (PTFE) at a weight ratio of 15:4:1. Lithium metal was used as the counter electrode and the reference electrode. The electrolyte was 1 M $LiPF_6$ dissolved in a 1:1:1 mixture of ethylene carbonate (EC), ethylene methyl carbonate (EMC), and dimethyl carbonate (DMC). The cells were assembled in a glovebox filled with high-purity argon. Discharge/charge measurements of the cells were performed at different current densities between the potentials of 0.01−3.00 V (vs Li^+/Li) under a LAND−CT2001A battery tester. The specific capacity was calculated according to the corresponding active material in each electrode, i.e., Fe_3O_4 for Fe_3O_4@C.

■ RESULTS AND DISCUSSION

Structure and Morphology. Fe_3O_4@C microcapsules were prepared by sintering a hydrothermally obtained precursor in argon. For the precursor, all the XRD patterns can be indexed to orthorhombic α-FeOOH (JCPDS Card No. 81-464) and no impurities are detected in the patterns (see Figure 1a). After the hydrothermal procedure, the XRD patterns do not change, except the higher background from 10° to 30° (see Figure 1b), which is due to the presence of amorphous carbon. When the above precursor was sintered at 500 °C for 4 h in flowing argon,
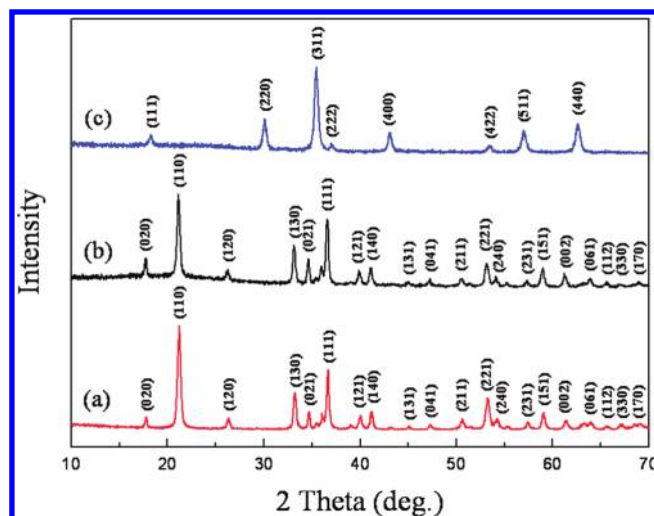

Figure 1. XRD patterns of α-FeOOH (spectrum a), α-FeOOH@C (spectrum b), and Fe_3O_4@C (spectrum c).
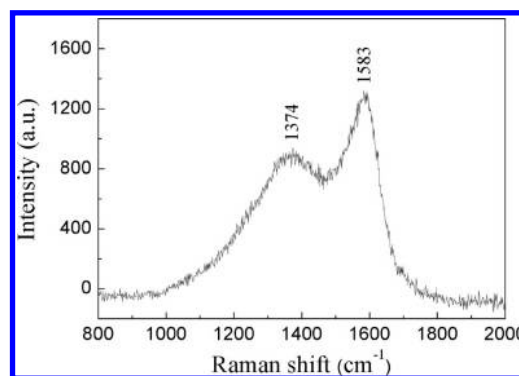

Figure 2. Raman spectrum of as-synthesized Fe_3O_4@C microcapsules.

the final product is determined to be Fe_3O_4 (JCPDS No. 19-629) (Figure 1c), and the EDS (shown in Figure S1 in the Supporting Information) illustrates that the product contains the elements iron, oxygen, and carbon, indicating the presence of carbon. Raman spectroscopy (Figure 2) also confirms the presence of carbon, with the "D" band appearing at ∼1374 cm^{-1} and the "G" band appearing at ∼1583 cm^{-1}. The peak intensity ratio between the D and G bands (I_D/I_G) is used as an index to estimate the degree of crystallization of carbon materials; the ordering degree of carbon increases as the I_D/I_G value decreases. Here, the I_D/I_G ratio of 0.7 indicates that the carbon has low crystallinity. Thermogravimetric (TG) analysis (see Figure S2 in the Supporting Information) determines that the carbon content is ∼32.8 wt %.

Typical SEM and TEM images provide insight into the morphology and structure of the samples. The α-FeOOH precursors are nanorods (Figure 3a) 20−100 nm in diameter and 100−500 nm in length. As shown in Figures 4a and 4b, the nanorod morphology is well preserved after a hydrothermal carbonization procedure and subsequent heating treatment; no obvious distinction occurs to the dimension and size. However, comparing the TEM images (see Figures 4c and 4d), we can clearly observe many irregular pores with diameters of 5−20 nm in Fe_3O_4 nanorods. However, the pore-size distribution curve obtained through the BJH method (Figure 5b) suggests that

706

dx.doi.org/10.1021/am1010095 |*ACS Appl. Mater. Interfaces* 2011, 3, 705–709
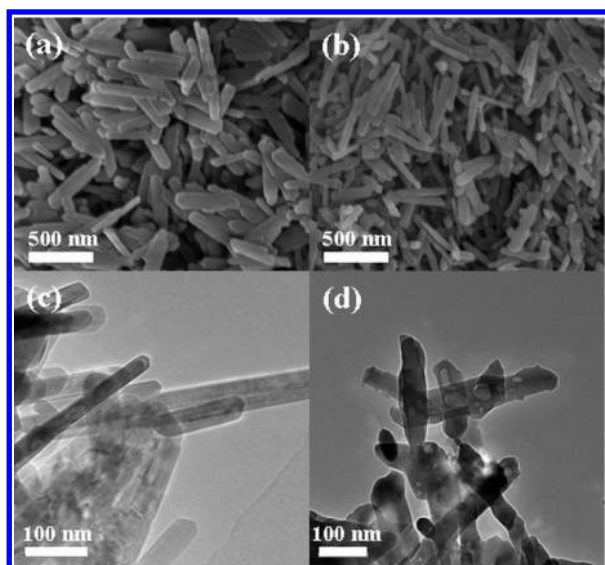
Figure 3. (Top) Typical SEM and (bottom) typical TEM images of α-FeOOH nanorods (panels a and c) and α-Fe$_2$O$_3$ nanorods (panels b and d).
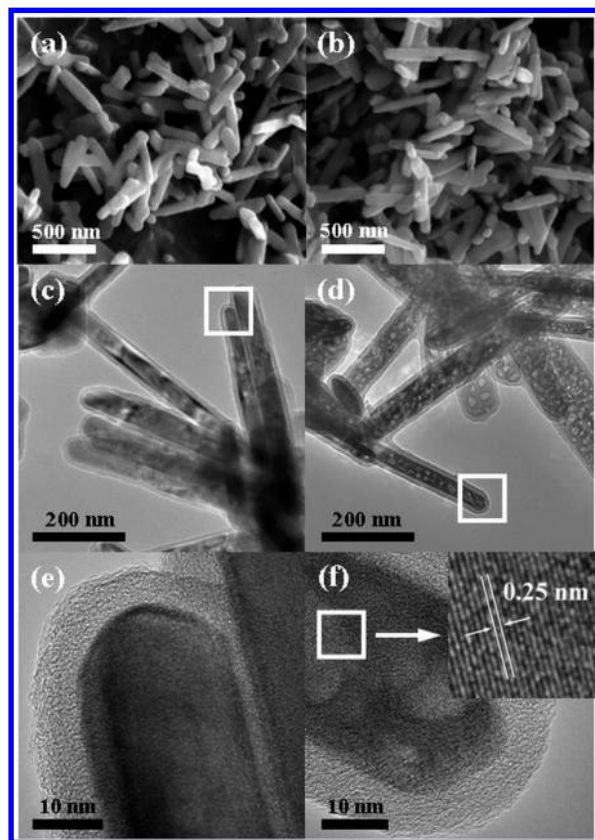
Figure 4. (Top) Typical SEM, (middle) TEM, and (bottom) HRTEM images of α-FeOOH@C nanorods (panels a, c, and e) and mesoporous Fe$_3$O$_4$@C nanorods (panels b, d, and f).

most pores show the sizes of ∼0.9 nm, which is attributed to the surface carbon layers; therefore, the pores observed in the TEM images are located in internal part of Fe$_3$O$_4$ cores, which are well-coated with carbon layers and cannot be detected through the N$_2$ physisorption measurements. The formation of mesopores is due to the removal of OH groups and the generation of CO$_2$, when
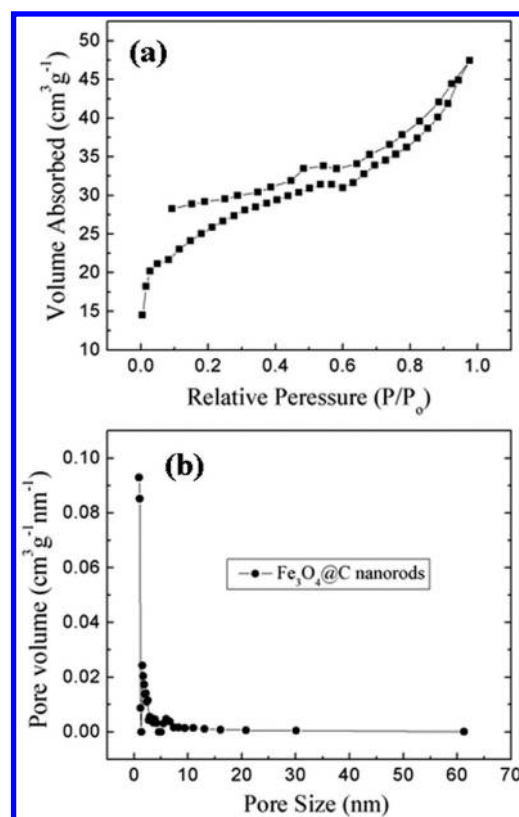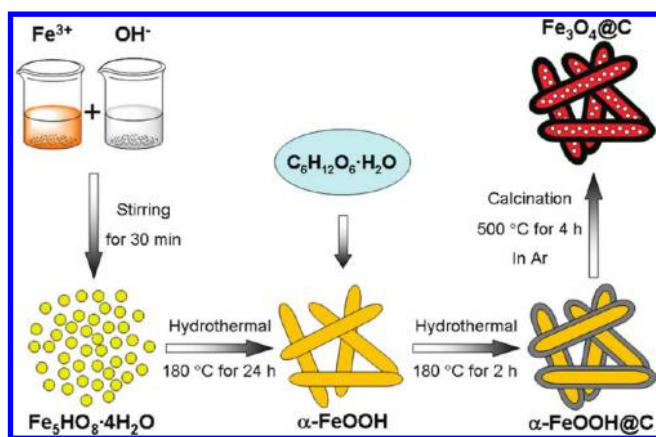

Figure 5. (a) N$_2$ adsorption−desorption isotherms and (b) pore-size distribution curves of Fe$_3$O$_4$@C microcapsules.

α-FeOOH is reduced to Fe$_3$O$_4$ by carbon. The representative high-resolution transmission electron microscopy (HRTEM) image (Figure 4f) shows the clear and continuous lattice fringes, indicating that Fe$_3$O$_4$ nanorods are highly crystalline single crystals. The lattice fringe pitch of 0.25 nm is magnified in the inset of Figure 4f and corresponds well with the *d*-spacing of the [311] reflections for Fe$_3$O$_4$, in agreement with the values of 2.532 Å obtained from the JCPDS database.[28] A uniform carbon layer with a thickness of ∼8 nm can be detected to coat the nanorods in the HRTEM images (Figures 4e and 4f) with no clear lattice fringe, indicating that the carbon is amorphous, which agrees well with the Raman spectrum (see Figure 2). The purpose of coating the nanorods with carbon is to reduce the risk of side reactions between active materials and the electrolyte, but not to shield the active materials from the outside environment. Accordingly, highly crystalline carbon increases the difficulty of lithium insertion and extraction, and low-crystallization amorphous carbon with many defects can allow Li ions to pass through carbon layers to react with inner Fe$_3$O$_4$ nanorods.[29]

Formation Mechanism. The formation process of amorphous carbon-coated mesoporous Fe$_3$O$_4$ nanorods involves four steps, as illustrated in Scheme 1. First, six-line ferrihydrite (Fe$_5$HO$_8$·4H$_2$O) nanodots were generated when Fe^{3+} was added to the excess-OH$^-$ solution, and then were converted to goethite nanodots with the prolonging of reaction time. Second, goethite nanodots aggregated and coarsened to goethite nanorods through the Ostwald ripening process.[30] The hydrothermal procedure at 180 °C for 24 h accelerated the aggregation and enhanced the crystallization and homogeneity of goethite nanorods. Third, goethite nanorods were coated with carbon for the carbonization of a glucose precursor via a hydrothermal process

Scheme 1. Illustration of the Formation Processes of Fe$_3$O$_4$@C Microcapsules

Figure 6. (a) Typical charge−discharge curves of Fe$_3$O$_4$@C microcapsule electrodes at a current density of 92.8 mA g^{-1} (0.1 C) for various cycles. (b) Cyclic performances of Fe$_3$O$_4$@C microcapsule electrode at different current densities of 92.8 mA g^{-1} (0.1 C), 185.6 mA g^{-1} (0.2 C), and 928 mA g^{-1} (1 C).

at 180 °C for 2 h. The surfaces of goethite nanorods with rich hydroxyl groups induced the in situ precipitation of carbonaceous units to form a uniform carbon shell.[31] Finally, carbon-coated Fe$_3$O$_4$ nanorods with irregular mesopores were yielded after sintering at 500 °C for 4 h in argon; these resemble microcapsules composed of inner mesoporous Fe$_3$O$_4$ nanorods and outer carbon encapsulation. The irregular mesopores formed from the removal of OH groups from α-FeOOH and the release of gases when carbon reduced Fe^{3+} to form Fe$_3$O$_4$:

$$12\alpha\text{-FeOOH} + C \rightarrow 4Fe_3O_4 + 6H_2O + CO_2$$
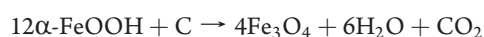
Without carbon, goethite was transformed to hematite (α-Fe$_2$O$_3$) (see Figure S3 in the Supporting Information) after heating at 500 °C for 4 h in argon, and the nanorod morphology was also maintained very well, but fewer irregular pores can be observed from the TEM image (see Figure 3d).

Electrochemical Performances. The electrochemical performances of as-prepared Fe$_3$O$_4$@C microcapsules were tested in Fe$_3$O$_4$/Li half cells. Figure 6a shows the charge−discharge curves for various cycles between 0.01 V and 3.00 V at a constant current density of 92.8 mA g^{-1} (0.1 C). The first discharge displays a specific capacity of ∼1540 mAh g^{-1}, while the capacity decreases to 1040 mAh g^{-1} in the second discharge. Such result is attributed to the formation of the SEI film and further lithium consumption via interfacial reactions, because of the charge separation at the metal/Li$_2$O phase boundary.[32] The voltage plateau at ∼0.75 V in the first cycle is different from those of other cycles at ∼1.0 V, indicating that irreversible reactions occurred in the first cycle. However, the electrode exhibited a high specific capacity of 1010 mAh g^{-1} after 50 cycles, which is still higher than the theoretical value of Fe$_3$O$_4$ (∼928 mAh g^{-1}). Similar results have been reported for many other transition-metal oxides.[33,34] Note that the final parts of the discharge curves are somewhat steep, which was also found in previous reports.[23,24] Steep discharge curves result from the nonequilibrium of two phases during electrochemical reactions. As for Fe$_3$O$_4$/C composites, extensive investigations are needed to completely elucidate the details.

The cyclic performances of Fe$_3$O$_4$@C microcapsule electrodes at different current densities are shown in Figure 6b. The Fe$_3$O$_4$@C microcapsules exhibit high retention efficiency with a stable specific capacity of 1010 mAh g^{-1} after 50 cycles at a

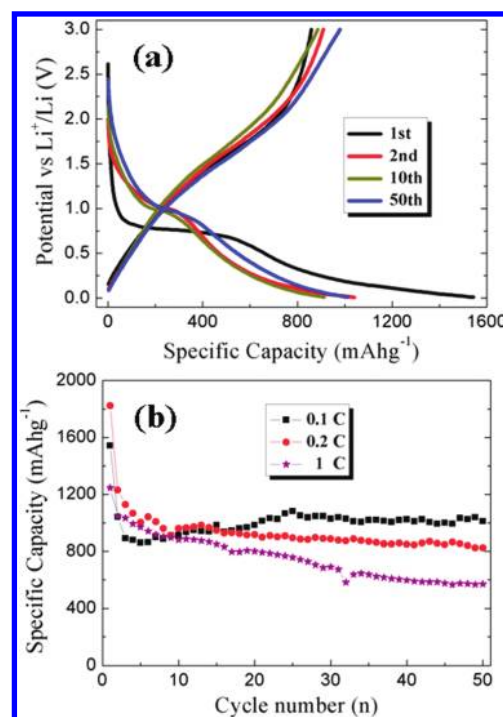current density of 92.8 mA g^{-1}, whereas the capacity of as-prepared α-Fe$_2$O$_3$ nanorods without carbon encapsulation is only 100 mAh g^{-1} (see Figure S4 in the Supporting Information). The visible capacity growth from the 5th cycle to the 25th cycle is due to the activation and stabilization of electrode materials. The specific capacities degrade with increasing current densities, but the high capacities of 800 mAh g^{-1} at 185.6 mA g^{-1} (0.2 C) and 600 mAh g^{-1} at 928 mA g^{-1} (1 C) can be retained after 50 cycles. SEM and TEM images (see Figure 7) demonstrate that the microcapsule structure was still maintained after 50 charge/discharge cycles only with volume expansion. Here, note that the above specific capacities correspond to the contribution of only Fe$_3$O$_4$. Actually, carbon also provides electrochemical capacities to the anodes (see Figure S5 in the Supporting Information). The average specific capacities corresponding to both Fe$_3$O$_4$ and C as active materials retain ∼800 mAh g^{-1} after 50 cycles at 92.8 mA g^{-1}. Compared to the same Fe$_3$O$_4$/carbon core−shell composites, except for the mesopores in Fe$_3$O$_4$ cores,[23,24] the Fe$_3$O$_4$@C microcapsule electrodes presented improved cyclic performances, probably due to the unique microstructures.

It is the coexistence of carbon encapsulation and mesopores in the proposed microcapsule-like structure that effectively improves the electrochemical performances of Fe$_3$O$_4$/C composites as LIB anode materials. The presence of amorphorous carbon layers on the surface of Fe$_3$O$_4$ nanorods reduces the risk of side reactions. The stable existence of a carbon shell can also restrict the volume variation of the electrode and avoid the pulverization of the electrode. The carbon layers with high electronic conductivity also act as efficient electrically conductive networks.[35] Moreover, the SEI film on the carbon shell can be
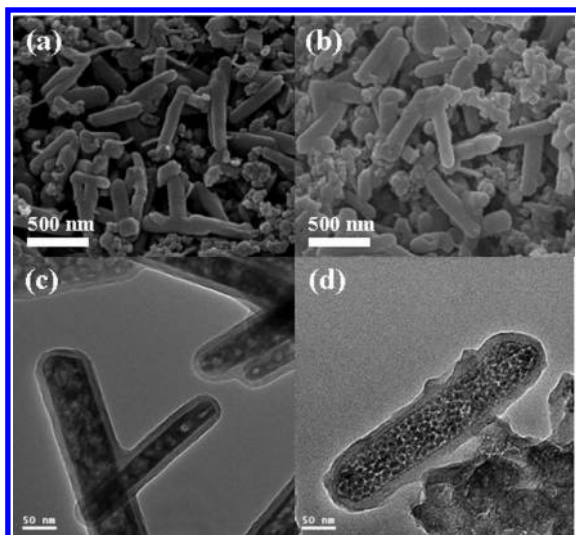
Figure 7. (Top) Typical SEM and (bottom) typical TEM images of Fe_3O_4@C microcapsules (a, c) before and (b, d) after 50 charge—discharge cycles at a current density of 92.8 mA g^{-1}.

maintained without decomposition during each charge/discharge process to consume the stored Li capacity.[36,37] The mesopores in the Fe_3O_4 nanorods play an important role in relieving the impact of volume change of active materials by providing the space for the volume expansion and contraction, and releasing the stress on the carbon shells. Without the buffering effects of mesopores, the carbon shells would suffer severe volumetric changes and might be destroyed during high-rate long charge/discharge cycles. For practical applications, further efforts are needed to reduce to the carbon coating content in the composites.

CONCLUSION

In summary, we prepared microcapsule-like composites of mesoporous Fe_3O_4 nanorods coated with amorphous carbon layers via two-step hydrothermal routes and a subsequent sintering process. The mesopores formed after the carbon coating procedure. When evaluated as anode materials for lithium-ion batteries (LIBs), the composites with the special structure displayed excellent electrochemical performances. The microcapsule concept of the combination of mesoporous core and carbon shell can be applied to other LIB materials.

ASSOCIATED CONTENT

ⓢ **Supporting Information.** EDS and TG analysis results of Fe_3O_4@C composites, XRD and electrochemical performances of Fe_2O_3 nanorods, and cyclic performances of hydrothermally obtained carbon. This material is available free of charge via the Internet at http://pubs.acs.org.

AUTHOR INFORMATION

Corresponding Author
*E-mail: zhouzhen@nankai.edu.cn.

ACKNOWLEDGMENT

REFERENCES

(1) Tarascon, J.-M.; Armand, M. *Nature* **2001**, *414*, 359.
(2) Armand, M.; Tarascon, J.-M. *Nature* **2008**, *451*, 652.
(3) Li, H.; Wang, Z. X.; Chen, L. Q.; Huang, X. J. *Adv. Mater.* **2009**, *21*, 1.
(4) Bruce, P. G.; Scrosati, B.; Tarascon, J.-M. *Angew. Chem., Int. Ed.* **2008**, *47*, 2930.
(5) Poizot, P.; Lauruelle, S.; Grugeon, S.; Dupont, L.; Tarascon, J.-M. *Nature* **2000**, *407*, 496.
(6) Chen, J.; Xu, L. N.; Li, W. Y.; Gou, X. L. *Adv. Mater.* **2005**, *17*, 582.
(7) Li, W. Y.; Xu, L. N.; Chen, J. *Adv. Funct. Mater.* **2005**, *15*, 851.
(8) Liu, L.; Li, Y.; Yuan, S. M.; Ge, M.; Ren, M. M.; Sun, C. S.; Zhou, Z. *J. Phys. Chem. C* **2010**, *114*, 251.
(9) Muraliganth, T.; Murugan, A. V.; Manthiram, A. *Chem. Commun.* **2009**, *47*, 7360.
(10) Nam, K. M.; Shim, J. H.; Han, D.-W.; Kwon, H. S.; Kang, Y.-M.; Li, Y.; Song, H.; Seo, W. S.; Park, J. T. *Chem. Mater.* **2010**, *22*, 4464.
(11) Kang, Y.-M.; Lee, S.-M.; Sung, M.-S.; Jeong, G.-J.; Kim, J.-S.; Kim, S.-S. *Electrochim. Acta* **2006**, *52*, 450.
(12) Kang, Y.-M.; Song, M.-S.; Kim, J.-H.; Kim, H.-S.; Park, M.-S.; Lee, J.-Y.; Liu, H. K.; Dou, S. X. *Electrochim. Acta* **2005**, *50*, 3667.
(13) Mitra, S.; Poizot, P.; Finke, A.; Tarascon, J.-M. *Adv. Funct. Mater.* **2006**, *16*, 2281.
(14) Taberna, P. L.; Mitra, S.; Poizot, P.; Simon, P.; Tarascon, J.-M. *Nat. Mater.* **2006**, *5*, 567.
(15) Debart, A.; Dupont, L.; Poizot, P.; Leriche, J. B.; Tarascon, J.-M. *J. Electrochem. Soc.* **2001**, *148*, A1266.
(16) Balaya, P.; Li, H.; Kienle, L.; Maier, J. *Adv. Funct. Mater.* **2003**, *13*, 621.
(17) Delmer, O.; Balaya, P.; Kienle, L.; Maier, J. *Adv. Mater.* **2008**, *20*, 501.
(18) Lou, X. W.; Li, C. M.; Archer, L. A. *Adv. Mater.* **2009**, *21*, 2536.
(19) Hu, Y. S.; Cakan, R. D.; Titirici, M. M.; Muller, J. O.; Schloge, R.; Antonietti, M.; Maier, J. *Angew. Chem., Int. Ed.* **2008**, *47*, 1645.
(20) Ren, M. M.; Zhou, Z.; Gao, X. P.; Peng, W. X.; Wei, J. P. *J. Phys. Chem. C* **2008**, *112*, 5689.
(21) Zhang, Y.; Sun, C. S.; Zhou, Z. *Electrochem. Commun.* **2009**, *11*, 1183.
(22) Su, L. W.; Zhou, Z.; Ren, M. M. *Chem. Commun.* **2010**, *46*, 2590.
(23) Liu, H.; Wang, G. X.; Wang, J. Z.; Wexler, D. *Electrochem. Commun.* **2008**, *10*, 1879.
(24) Zhang, W. M.; Wu, X. L.; Hu, J. S.; Guo, Y. G.; Wan, L. J. *Adv. Funct. Mater.* **2008**, *18*, 3941.
(25) Piao, Y. Z.; Kim, H. S.; Sung, Y. E.; Hyeon, T. *Chem. Commun.* **2010**, *46*, 118.
(26) Ban, C. M.; Wu, Z. C.; Gillaspie, D. T.; Chen, L.; Yan, Y. F.; Blackburn, J. L.; Dillon, A. C. *Adv. Mater.* **2010**, *22*, E145.
(27) Zhou, H. S.; Li, D. L.; Hibino, M.; Honma, I. *Angew. Chem., Int. Ed.* **2005**, *44*, 797.
(28) Jiao, F.; Jumas, J. -C.; Womes, M.; Chadwick, A. V.; Harrison, A.; Bruce, P. G. *J. Am. Chem. Soc.* **2006**, *128*, 12905.
(29) Cheng, L.; Li, X. L.; Liu, H. J.; Xiong, H. M.; Zhang, P .W.; Xia, Y. Y. *J. Electrochem. Soc.* **2007**, *154*, A692.
(30) Burleson, D. J.; Penn, R. L. *Langmuir* **2006**, *22*, 402.
(31) Sun, X. M.; Liu, J. F.; Li, Y. D. *Chem. Mater.* **2006**, *18*, 3486.
(32) Jamnik, J.; Maier, J. *Phys. Chem. Chem. Phys.* **2003**, *5*, 5215.
(33) Lou, X. W.; Deng, D.; Lee, J. Y.; Archer, L. A. *J. Mater. Chem.* **2008**, *18*, 4397.
(34) Chou, S. L.; Wang, J. Z.; Wexler, D.; Konstantinov, K.; Zhong, C.; Liu, H. K.; Dou, S. X. *J. Mater. Chem.* **2010**, *20*, 2092.
(35) Guo, Y. G.; Hu, Y. S.; Sigle, W.; Maier, J. *Adv. Mater.* **2007**, *19*, 2087.
(36) Hu, J.; Li, H.; Huang, X.; Chen, L. *Solid State Ionics* **2006**, *177*, 2791.
(37) Needham, S. A.; Wang, G. X.; Konstantinov, K.; Tournayre, Y.; Lao, Z.; Liu, H. K. *Electrochem. Solid-State Lett.* **2006**, *9*, A3153.